EUROPEAN ORGANIZATION FOR NUCLEAR RESEARCH

CERN-PH-EP/2005-013
April 4, 2005

Neutral-Current Four-Fermion Production in e^+e^- Interactions at LEP

The L3 Collaboration

Abstract

Neutral-current four-fermion production, $e^+e^- \to f\bar{f}f'\bar{f}'$, is studied in 0.7 fb^{-1} of data collected with the L3 detector at LEP at centre-of-mass energies $\sqrt{s} = 183 - 209$ GeV. Four final states are considered: $q\bar{q}\nu\bar{\nu}$, $q\bar{q}\ell^+\ell^-$, $\ell^+\ell^-\ell'^+\ell'^-$ and $\ell^+\ell^-\nu\bar{\nu}$, where ℓ denotes either an electron or a muon. Their cross sections are measured and found to agree with the Standard Model predictions. In addition, the $e^+e^- \to Z\gamma^* \to f\bar{f}f'\bar{f}'$ process is studied and its total cross section at the average centre-of-mass energy $\langle\sqrt{s}\rangle = 196.6$ GeV is found to be $0.29 \pm 0.05 \pm 0.03$ pb, where the first uncertainty is statistical and the second systematic, in agreement with the Standard Model prediction of 0.22 pb. Finally, the mass spectra of the $q\bar{q}\ell^+\ell^-$ final states are analysed to search for the possible production of a new neutral heavy particle, for which no evidence is found.

Submitted to *Phys. Lett. B*

1 Introduction

The centre-of-mass energy, $\sqrt{s}$, of the LEP e^+e^- collider reached 209 GeV, allowing the study of four-fermion production mediated by the exchange of real and virtual gauge-bosons. Four-fermion events are classified as charged-current processes or neutral-current processes [1, 2]. The former proceed through the exchange of W bosons, while the latter comprise the exchange of both Z bosons and off-mass-shell photons.

The L3 collaboration has investigated both charged-current processes, in particular W-boson pair production [3] and single W-boson production [4], and neutral-current processes, with Z-boson pair production [5] and single Z-boson production [6]. Reference 7 provides a comprehensive bibliography of these studies at LEP. This Letter extends previous studies, focused on the signature of boson pairs or a single boson and missing energy, to a general analysis of neutral-current processes, $e^+e^- \to f\bar{f}f'\bar{f}'$, with either high-mass or low-mass fermion pairs. The special case of events with a Z boson and an off-mass-shell photon, $e^+e^- \to Z\gamma^* \to f\bar{f}f'\bar{f}'$, is also considered. Figure 1 presents some of the Feynman diagrams responsible for neutral-current four-fermion production. In the following, four processes with different combinations of quarks, leptons and neutrinos in the final state are considered: $e^+e^- \to q\bar{q}\nu\bar{\nu}$, $e^+e^- \to q\bar{q}\ell^+\ell^-$, $e^+e^- \to \ell^+\ell^-\nu\bar{\nu}$ and $e^+e^- \to \ell^+\ell^-\ell'^+\ell'^-$, where ℓ denotes either an electron[1)] or a muon. Events with tau leptons are considered as background.

High-resolution studies of four-fermion events are also sensitive to manifestations of new physics, and the mass spectra of events from the $e^+e^- \to q\bar{q}\ell^+\ell^-$ process are investigated to search for new neutral heavy particles decaying into hadrons.

L3 results on neutral-current four-fermion production in a smaller data sample obtained at lower values of $\sqrt{s}$ are discussed in References 8 and 9. A study of the $e^+e^- \to q\bar{q}\ell^+\ell^-$ process by the OPAL collaboration is described in Reference 10.

Process	Signal definition
$e^+e^- \to q\bar{q}\nu\bar{\nu}$	$m_{q\bar{q}} > 10$ GeV
$e^+e^- \to q\bar{q}\ell^+\ell^-$	$\lvert\cos\theta_\ell\rvert < 0.95$, $m_{\ell^+\ell^-} > 5$ GeV, $m_{q\bar{q}} > 10$ GeV
$e^+e^- \to \ell^+\ell^-\nu\bar{\nu}$	$\lvert\cos\theta_\ell\rvert < 0.95$, $m_{\ell^+\ell^-} > 5$ GeV, $m_{\ell\nu} \notin [70\text{ GeV}, 90\text{ GeV}]$
$e^+e^- \to \ell^+\ell^-\ell'^+\ell'^-$	$\lvert\cos\theta_\ell\rvert < 0.95$, $\lvert\cos\theta_{\ell'}\rvert < 0.95$, $m_{\ell^+\ell^-} > 5$ GeV, $m_{\ell'^+\ell'^-} > 5$ GeV, $m_{\ell^\pm\ell'^\mp} > 5$ GeV if ℓ and ℓ' have same flavour
$e^+e^- \to Z\gamma^* \to f\bar{f}f'\bar{f}'$	$m_{f\bar{f}} \in [m_Z - 2\Gamma_Z, m_Z + 2\Gamma_Z]$ and $m_{f'\bar{f}'} \notin [m_Z - 2\Gamma_Z, m_Z + 2\Gamma_Z]$ or $m_{f\bar{f}} \notin [m_Z - 2\Gamma_Z, m_Z + 2\Gamma_Z]$ and $m_{f'\bar{f}'} \in [m_Z - 2\Gamma_Z, m_Z + 2\Gamma_Z]$

Table 1: Signal definition for neutral-current four-fermion final states

The studies of four-fermion final states are restricted to a limited part of the full phase space as described in Table 1. These signal-definition criteria have multiple purposes. Cuts on the cosine of the angle between the leptons and the beam axis, $|\cos\theta_\ell|$ and $|\cos\theta_{\ell'}|$, restrict the comparison between data and predictions to regions compatible with the geometrical coverage of the detector, thus avoiding large extrapolation factors. Cuts on the masses of the fermion-antifermion pairs, $m_{\ell^+\ell^-}$, $m_{\ell'^+\ell'^-}$ and $m_{q\bar{q}}$, remove contributions of strongly-interacting resonances in the low-mass regions. If four same-flavour leptons are produced in the $e^+e^- \to \ell^+\ell^-\ell'^+\ell'^-$ process, an additional mass cut is applied to account for all possible

[1)] Throughout this Letter the term "electron" stands for both electrons and positrons.

lepton combinations. The $e^+e^- \to \ell^+\ell^-\nu\bar{\nu}$ process is mostly due to charged-current W-boson pair production, studied in detail elsewhere [3]. A cut is applied on the lepton-neutrino mass, $m_{\ell\nu}$, to reduce the contribution of W bosons and enhance that of neutral-current four-fermion production.

Two additional phase-space criteria, also listed in Table 1, are applied to increase the relative contribution from the $e^+e^- \to Z\gamma^* \to f\bar{f}f'\bar{f}'$ process. The mass of one of the fermion-antifermion pairs is required to be in the range $m_Z \pm 2\Gamma_Z$, while the mass of the other pair is required to be outside this range, where $m_Z = 91.19$ GeV [11] and $\Gamma_Z = 2.49$ GeV [11] are the Z-boson mass and width, respectively.

2 Data and Monte Carlo samples

The full data-sample collected at high centre-of-mass energies with the L3 detector [12] is investigated. It amounts to 673.4 pb^{-1} of integrated luminosity for $\sqrt{s} = 182.7 - 209.2$ GeV, with a luminosity-weighted average centre-of-mass energy $\langle\sqrt{s}\rangle = 196.6$ GeV. The data were collected around eight average $\sqrt{s}$ values, listed in Table 2 together with the corresponding integrated luminosities. The 55.4 pb^{-1} of data collected at $\sqrt{s} = 182.7$ GeV, already discussed in Reference 9, are re-analysed within the signal definitions discussed above.

In order to optimise the event selection and calculate the signal efficiencies, four-fermion events are generated with the EXCALIBUR [13] Monte Carlo program in a phase space larger than that of the signal definition criteria of Table 1. These cuts are applied on generated quantities and the selected events are considered as signal, while the remaining ones are treated as background. EXCALIBUR is also used to model four-fermion background from the $e^+e^- \to \tau^+\tau^- f\bar{f}$ and $e^+e^- \to We\nu$ processes. Additional four-fermion background is due to W-boson pair production and subsequent decay into fully-hadronic or semi-leptonic final states. This process is modelled with the KORALW [14] Monte Carlo program. The background from fermion pair-production, $e^+e^- \to q\bar{q}$, $e^+e^- \to \tau^+\tau^-$ and $e^+e^- \to \mu^+\mu^-$, is described by KK2f [15]. Bhabha scattering is described with BHAGENE [16] and BHWIDE [17]. The $e^+e^- \to e^+e^-\gamma$ process with high transverse-momentum photons and low polar-angle electrons is simulated with TEEGG [18]. Events with multiple hard-photon production are generated with GGG [19]. Hadron and lepton production in two-photon collisions are modelled with PHOJET [20] and DIAG36 [21], respectively.

The L3 detector response is simulated using the GEANT [22] program which takes into account the effects of energy loss, multiple scattering and showering in the detector. GHEISHA [23] is used for the simulation of hadronic interactions. Time-dependent detector efficiencies, as monitored during the data-taking period, are included in the simulations.

The signal cross sections are calculated with the GRC4F [24] Monte Carlo program which, unlike EXCALIBUR, includes fermion masses. About twenty thousand events are generated at each value of $\sqrt{s}$ for each possible flavour combination. The numbers of events satisfying the criteria in Table 1 and their weights are then used to calculate the signal cross sections, listed in Table 3. The cross sections for the $e^+e^- \to Z\gamma^* \to f\bar{f}f'\bar{f}'$ processes are extracted for each final state by applying the additional cuts in Table 1, with the results listed in Table 4.

Small differences between the GRC4F and the EXCALIBUR modelling of the $e^+e^- \to f\bar{f}f'\bar{f}'$ process have a negligible impact on the measurements described in the following.

3 Event selection

The event selection [25] is similar to that devised for the study of Z-boson pair production [5]. Events which contain electrons, muons or hadronic jets are selected and these objects are then combined to construct kinematic variables to isolate the neutral-current four-fermion signal from the two-fermion, four-fermion and two-photon backgrounds.

Electrons are identified by requiring a well-isolated electromagnetic cluster in the electromagnetic calorimeter with an associated track in the tracking chamber. To increase efficiency, this track-matching requirement is relaxed by some selections.

Muons are reconstructed from correlated tracks in the muon spectrometer and the central tracker which are in time with the beam crossing. Calorimetric clusters compatible with a minimum ionising particle with an associated track in the central tracker are also accepted.

Quark fragmentation and hadronisation yield a high multiplicity of calorimetric clusters and charged tracks. These are grouped into jets by means of the DURHAM algorithm [26].

Fermion-antifermion pairs can originate from a Z boson or, for charged fermions, from an off-mass-shell photon. In the first case, the pair is characterised by high mass, while in the second case it has most likely a low mass. Appropriate selections for these two cases are implemented.

Typical selection variables are: the visible energy of the event, $E_{\rm vis}$; the transverse, $p_{\rm t}$, and longitudinal, $p_{\parallel}$, components of the vectorial sum of the momenta of all objects in the event; the missing momentum, $p_{\rm mis}$, and the angles between two jets or two leptons in space, $\Delta\psi$, or in the plane transverse to the beam axis, $\Delta\phi$.

The data sample spans a $\sqrt{s}$ range of about 25 GeV, which results in appreciable differences in the kinematics of the signals. The selection criteria are optimised to reflect these differences and change over the $\sqrt{s}$ range.

Some aspects of the different selections are described in the following, while their yields are summarised in Table 3.

3.1 The $\mathrm{q\bar{q}}\nu\bar{\nu}$ channel

The signature of the $\mathrm{e^+e^-} \to \mathrm{q\bar{q}}\nu\bar{\nu}$ process is two hadronic jets and missing energy mostly due to the production of a Z boson decaying into neutrinos. The most important background is W-boson pair production.

High-multiplicity events are selected and reconstructed as two jets. No electrons or muons with energies above 20 GeV are allowed in order to reduce the background from W-boson pair production and subsequent semi-leptonic decay. Events with photons with energy above 20 GeV are rejected so as to reduce background from the $\mathrm{e^+e^-} \to \mathrm{q\bar{q}}$ process with a hard initial-state-radiation (ISR) photon. The background from hadron production in two-photon collisions is suppressed by limiting the energy deposition in the low-angle calorimeters and by rejecting events with a two-jet mass, $m_{\rm qq}$, below 10 GeV. A low-mass selection is applied for $m_{\rm qq} < 50$ GeV and a high-mass selection otherwise.

The low-mass selection removes background from hadron production in two-photon collision by requiring at least one jet to point more than 0.3 rad away from the beam axis. The $\mathrm{e^+e^-} \to \mathrm{q\bar{q}}$ process results in two back-to-back jets in the plane transverse to the beams and, if no ISR occurred, in two jets which are also back-to-back in space. It is strongly suppressed by requiring $\Delta\phi < 3\,\mathrm{rad}$ and $\Delta\psi < 3\,\mathrm{rad}$. The requirements $\Delta\phi > 1.8\,\mathrm{rad}$ and $\Delta\psi > 1.8\,\mathrm{rad}$ remove background from the $\mathrm{e^+e^-} \to \mathrm{We}\nu$ process and semi-leptonic decays of W-boson pairs as the W-boson boost results in opening angles smaller than those for the signal. Large missing

momentum is due to the production of a Z boson and is tagged by requiring $p_{\rm mis} > 0.3\ \sqrt{s}$ and $p_{\rm t} > 0.3\sqrt{s}$.

The high-mass selection accepts events with a higher multiplicity and a missing mass, $m_{\nu\nu} = \sqrt{(\sqrt{s} - E_{\rm vis})^2 - p_{\rm mis}^2}$, compatible with $m_{\rm Z}$, 78 GeV $< m_{\nu\nu} <$ 115 GeV. Background from W-boson pair production and the $\rm e^+e^- \to q\bar{q}$ process is reduced by requiring 8 GeV $< p_{\rm t} <$ 40 GeV. The normal to the plane of the two jets must not point more than 1.5 rad away from the beam axis. In addition, the event thrust must be greater than $0.78 - 0.88$ and $\Delta\psi > 2 - 2.5$ rad, depending on $\sqrt{s}$. The $\rm e^+e^- \to q\bar{q}$ process with hard ISR photons is further reduced by requiring $p_{\parallel} < 30 - 42$ GeV.

Figure 2a shows the distribution of $\Delta\phi$ for both the low- and high-mass selections. The residual background is mostly due to W-boson pair production and the $\rm e^+e^- \to We\nu$ process.

3.2 The $\rm q\bar{q}\ell^+\ell^-$ channel

The signature of the $\rm e^+e^- \to q\bar{q}\ell^+\ell^-$ process is two hadronic jets and either an electron or a muon pair. This signature can also arise from four-fermion events outside the signal definition. Other sources of background are W-boson pair production and the $\rm e^+e^- \to q\bar{q}$ process with leptons coming from heavy-quark decays.

High-multiplicity events with two electrons or two muons are selected and the remaining calorimetric clusters are reconstructed as two jets. The measured energies and momenta of the two jets and the two leptons are varied within their resolutions to best fit the hypotheses of energy and momentum conservation. This kinematic fit improves the resolution of the jet-energy measurements.

Events with W-boson pair production and semi-leptonic decay have missing momentum due to the neutrinos and are suppressed by requiring $p_{\rm t}/E_{\rm vis} < 0.35$ and $p_{\parallel}/E_{\rm vis} < 0.35$. A low-mass selection is applied if 500 GeV$^2 < m_{\rm qq} \times m_{\ell\ell} <$ 4000 GeV^2, where $m_{\rm qq}$ is the two-jet mass and $m_{\ell\ell}$ the mass of the lepton pair. A high-mass selection covers the range $m_{\rm qq} \times m_{\ell\ell} >$ 4000 GeV^2. Events with $m_{\rm qq} \times m_{\ell\ell} <$ 500 GeV^2 exhibit a large background contamination and are not further considered. The selection criteria depend on the flavour of the leptons and on $\sqrt{s}$.

In order to reduce the background from W-boson pair production, the low-mass analysis requires $p_{\rm t}/E_{\rm vis} < 0.12 - 0.14$ for electrons and $p_{\rm t}/E_{\rm vis} < 0.22 - 0.30$ for muons. The energy of the most energetic lepton, E_1, is required to satisfy $E_1/\sqrt{s} > 0.12 - 0.15$ in order to remove leptons from heavy-quark decays. For electrons, the energy of the least energetic lepton, E_2, must satisfy $E_2/\sqrt{s} > 0.07 - 0.15$. The high-mass analysis requires $E_2/\sqrt{s} > 0.06 - 0.10$ and $p_{\rm t}/E_{\rm vis} < 0.11 - 0.14$ for electrons and $E_1/\sqrt{s} > 0.10 - 0.16$ and $E_{\rm vis}/\sqrt{s} > 0.5 - 0.7$ for muons. Figures 2b and 2c, show the distributions of $p_{\rm t}/E_{\rm vis}$ and $E_1/\sqrt{s}$.

The residual background in both channels is due to events from four-fermion production outside the signal definition, from W-boson pair production and from the $\rm e^+e^- \to q\bar{q}$ process.

3.3 The $\ell^+\ell^-\nu\bar{\nu}$ channel

The signature of the $\rm e^+e^- \to \ell^+\ell^-\nu\bar{\nu}$ process is an electron or muon pair and large missing energy, mostly due to a Z boson decaying into neutrinos. The most important backgrounds are lepton pair production with a hard ISR photon and W-boson pair production.

Events with just one or two tracks associated to two identified electrons or muons are selected. To reduce background from annihilation and two-photon lepton pair production, no large energy deposition is allowed in the low polar-angle calorimeters. Events with $m_{\ell\ell} <$

10 GeV are removed from the sample. The remaining events are considered by three overlapping selections, according to the value of $m_{\ell\ell}$. Background from lepton pair production results in low-p_{t} events with back-to-back leptons and is reduced by requiring $p_{\mathrm{t}}/\sqrt{s} > 0.1 - 0.3$ and $\Delta\phi < 2.6 - 3.1$ rad as shown in Figure 2d. The background is strongly suppressed by requiring the recoil mass to be compatible with m_{Z}. Finally, the signal purity is enhanced by requiring $E_{\mathrm{vis}}/\sqrt{s} > 0.4 - 0.5$ and $E_1/\sqrt{s} > 0.2 - 0.4$.

The remaining background is almost entirely due to $\mathrm{e^+e^-} \to \ell^+\ell^-\nu\bar{\nu}$ events outside the signal definition criteria.

3.4 The $\ell^+\ell^-\ell'^+\ell'^-$ channel

The signature of the $\mathrm{e^+e^-} \to \ell^+\ell^-\ell'^+\ell'^-$ process is four leptons of which at least one pair originates from a Z boson or a low-mass virtual photon. These configurations are found in background from four-fermion events outside the signal definition criteria and lepton pair production with additional radiative photons, which mimic electrons in the detector.

Events with three or four tracks and four identified leptons are selected if $E_{\mathrm{vis}}/\sqrt{s} > 0.4$. All same-flavour lepton pairs are considered and their mass is calculated. If at least one pair has a mass above 40 GeV, the event is considered by a high-mass selection which starts from the lepton pair with mass closer to m_{Z}. A low-mass selection, aimed to identify events with a lepton pair originating from a low-mass off-mass-shell photon, is applied if at least one lepton pair has a mass below 60 GeV. The low-mass selection starts from the lepton pair with the lowest mass. An event can be considered and selected by both selections.

The high-mass selection requires the lepton pair to have 1.55 rad $< \Delta\psi <$ 3.10 rad, where the upper cut removes non-radiative fermion-pair events. The other two leptons must satisfy 0.1 rad $< \Delta\phi <$ 2.3 rad. Radiative lepton-pair production is further suppressed by requiring $p_{\parallel}/\sqrt{s} < 0.4$. Four-fermion background is reduced by requiring the masses of both pairs to be below 120 GeV.

The low-mass selection requires the lepton pair to have 0.1 rad $< \Delta\psi <$ 2.8 rad, while the two other leptons must satisfy $\Delta\phi <$ 1.0 rad and 1.45 rad $< \Delta\psi <$ 3.05 rad. Radiative lepton-pair production is suppressed by requiring $p_{\parallel}/\sqrt{s} < 0.36$, $p_{\mathrm{t}}/\sqrt{s} > 0.06$ and by upper cuts on the lepton energies. Four-fermion events outside the signal definition are removed by requiring the mass of the second pair to be in the range $14 - 152$ GeV.

The residual background originates in equal parts from lepton pair production and four-fermion events outside the signal definition criteria. Some contribution from lepton production in two-photon collisions is observed for final states with electrons.

4 Results

4.1 The $\mathrm{e^+e^-} \to f\bar{f}f'\bar{f}'$ process

Figure 3 presents two-dimensional plots of the $m_{\nu\nu}$ and m_{qq} masses for the $\mathrm{q\bar{q}}\nu\bar{\nu}$ final state and the $m_{\ell\ell}$ and m_{qq} masses for the $\mathrm{q\bar{q}}\ell^+\ell^-$ final states. The data exhibit contributions from Z-boson pair production, final states with a Z boson and an off-mass-shell virtual photon and the continuum. A good agreement is observed with the Monte Carlo predictions, for the $\mathrm{q\bar{q}}\nu\bar{\nu}$ and $\mathrm{q\bar{q}e^+e^-}$ final states, with some fluctuations for the $\mathrm{q\bar{q}}\mu^+\mu^-$ final state.

The cross sections for neutral-current four-fermion production are derived from the $m_{\ell\ell}$ spectra for all channels with leptons and the m_{qq} spectrum for the $\mathrm{q\bar{q}}\nu\bar{\nu}$ final state, shown in

Figure 4. The background level and shape is fixed to the Monte Carlo predictions, and the $e^+e^- \to f\bar{f}f'\bar{f}'$ normalisation is then derived from the data. Table 3 compares the measured and expected cross sections, determined as the luminosity-weighted average of the cross sections at each of the average centre-of-mass energies listed in Table 2. A good agreement is observed.

Several possible sources of systematic uncertainties are considered as summarised in Table 5. The jet and lepton identification and reconstruction are affected by the energy scale of the calorimeters and the accuracy of the track measurements. The analysis is repeated by varying the energy scale by $\pm 2\%$ and modifying the lepton selection criteria. The differences are considered as systematic uncertainties.

Monte Carlo modelling of the detector response is in general accurate. Possible systematic uncertainties could arise from distortions in the modelling of tails of distributions used in the event selection. These are addressed by varying the selection criteria on the variables susceptible to remove the largest part of the background by an amount compatible with their resolution. The measurements of the cross sections are repeated and largest variations are assigned as systematic uncertainties.

Small effects from the limited signal and background Monte Carlo statistics are also considered as systematic uncertainties.

Finally, the uncertainties of the background normalisations are propagated to the measured cross sections. A variation of $\pm 10\%$ is assumed for neutral-current four-fermion events generated with EXCALIBUR which fail the signal identification criteria and for the $e^+e^- \to We\nu$ process, $\pm 2\%$ on fermion pair production, $\pm 0.5\%$ on W-boson pair production, and $\pm 25\%$ and $\pm 50\%$ on lepton and hadron production in two-photon collisions, respectively.

4.2 The $e^+e^- \to Z\gamma^* \to f\bar{f}f'\bar{f}'$ process

The cross sections of the $e^+e^- \to Z\gamma^* \to f\bar{f}f'\bar{f}'$ process are determined with the same procedure as described above. Signal Monte Carlo events are subjected to the additional signal definition criteria for the $e^+e^- \to Z\gamma^* \to f\bar{f}f'\bar{f}'$ process described in Table 1. The selected events are treated as the $e^+e^- \to Z\gamma^* \to f\bar{f}f'\bar{f}'$ signal, illustrated in Figure 4. Events which fail these criteria are considered as an additional background and their cross section is fixed to the predictions. The cross sections measured for each channel are presented in Table 4. Systematic uncertainties are assessed as for neutral-current four-fermion production and listed in Table 5.

By combining the five different channels, the total $e^+e^- \to Z\gamma^* \to f\bar{f}f'\bar{f}'$ cross section at $\langle\sqrt{s}\rangle = 196.6$ GeV is determined to be $0.29 \pm 0.05 \pm 0.03$ pb, where the first uncertainty is statistical and the second systematic, to be compared with the GRC4F prediction of 0.22 pb.

4.3 Production of neutral heavy particles

Figures 5a and 5c present the spectra of the mass recoiling against the electron or muon pairs, respectively, while Figures 5e presents their sum. A new, neutral, heavy particle decaying into hadrons would manifest as a peak in these distributions. All distributions agree with the Monte Carlo predictions: apart from the Z-boson peak, no other significant structure is observed. The study is narrowed to the case in which the mass of the lepton pair is compatible with $|m_{\ell\ell} - m_Z| < 2\Gamma_Z$. Again, no significant deviations from the Standard Model predictions are observed, as presented in Figures 5b, 5d and 5f.

Summary

The high energies and high luminosity achieved by LEP have allowed detailed studies of four-fermion production. Previous L3 studies involving single and pair production of W and Z bosons are complemented with a study of events from inclusive four-fermion neutral-current production, $e^+e^- \to f\bar{f}f'\bar{f}'$, and from the $e^+e^- \to Z\gamma^* \to f\bar{f}f'\bar{f}'$ process. Four different final states are considered. Their cross sections are measured and found to agree with the Standard Model predictions, as shown in Table 3, Table 4 and Figure 6 for the $e^+e^- \to q\bar{q}\nu\bar{\nu}$, $e^+e^- \to q\bar{q}\ell^+\ell^-$ and $e^+e^- \to Z\gamma^* \to f\bar{f}f'\bar{f}'$ processes. The combined statistical and systematic accuracy of the $e^+e^- \to Z\gamma^* \to f\bar{f}f'\bar{f}'$ cross section measurement is 15%. No evidence is found for a new neutral hadronic-decaying heavy particle produced in four-fermion events.

References

[1] D. Bardin *et al.*, Nucl. Phys. (Proc. Suppl.) **B 37** (1994) 148;
F.A. Berends *et al.*, Nucl. Phys. (Proc. Suppl.) **B 37** (1994) 163.

[2] *Physics at LEP 2* Report CERN 96-01 (1996), eds G. Altarelli, T. Sjöstrand, F. Zwirner.

[3] L3 Collab., P. Achard *et al.*, Phys. Lett. **B 600** (2004) 22.

[4] L3 Collab., P. Achard *et al.*, Phys. Lett. **B 547** (2002) 151.

[5] L3 Collab., P. Achard *et al.*, Phys. Lett. **B 572** (2003) 133.

[6] L3 Collab., P. Achard *et al.*, Phys. Lett. **B 561** (2003) 73.

[7] D. Abbaneo *et al.*, *A combination of preliminary electroweak measurements and constraints on the Standard Model*, preprint hep-ex/0412015 (2004), Chapter 10.

[8] L3 Collab., M. Acciarri *et al.*, Phys. Lett. **B 413** (1997) 191.

[9] L3 Collab., M. Acciarri *et al.*, Phys. Lett. **B 450** (1999) 281.

[10] OPAL Collab., G. Abbiendi *et al.*, Phys. Lett. **B 544** (2002) 259.

[11] Particle Data Group, S. Eidelman *et al.*, Phys. Lett. **B 592** (2004) 1.

[12] L3 Collab., B. Adeva *et al.*, Nucl. Inst. Meth. **A 289** (1990) 35;
L3 Collab., O. Adriani *et al.*, Physics Reports **236** (1993) 1;
I.C. Brock *et al.*, Nucl. Instr. and Meth. **A 381** (1996) 236;
M. Chemarin *et al.*, Nucl. Inst. Meth. **A 349** (1994) 345;
M. Acciarri *et al.*, Nucl. Inst. Meth. **A 351** (1994) 300;
A. Adam *et al.*, Nucl. Inst. Meth. **A 383** (1996) 342;
G. Basti *et al.*, Nucl. Inst. Meth. **A 374** (1996) 293.

[13] EXCALIBUR version 1.11 is used.
F.A. Berends, R. Kleiss and R. Pittau, Comp. Phys. Comm. **85** (1995) 437.

[14] KORALW version 1.51 is used.
S. Jadach *et al.*, Comp. Phys. Comm. **119** (1999) 272.

[15] KK2f versions 4.14 and 4.19 are used.
S. Jadach *et al.*, Comp. Phys. Comm. **130** (2000) 260;
S. Jadach *et al.*, Phys. Rev. **D 63** (2001) 113009.

[16] BHAGENE version 3.0 is used.
J.H. Field, Phys. Lett. **B 323** (1994) 432;
J.H. Field and T. Riemann, Comp. Phys. Comm. **94** (1996) 53.

[17] BHWIDE version 1.01 is used.
S. Jadach *et al.*, Phys. Rev. **D 40** (1989) 3582,
S. Jadach *et al.*, Comp. Phys. Comm. **70** (1992) 305,
S. Jadach *et al.*, Phys. Lett. **B 390** (1997) 298.

[18] TEEGG version 7.1 is used.
D. Karlen, Nucl. Phys. **B 289** (1987) 23.

[19] GGG Monte Carlo:
F.A. Berends and R. Kleiss, Nucl. Phys. **B 186** (1981) 22.

[20] PHOJET version 1.05 is used.
R. Engel, Z. Phys. **C 66** (1995) 203;
R. Engel and J. Ranft, Phys. Rev. **D 54** (1996) 4244.

[21] DIAG36 version 1.0 is used.
F.A. Berends *et al.*, Nucl. Phys. **B 253** (1985) 441.

[22] GEANT version 3.15 is used.
R. Brun *et al.*, preprint CERN-DD/EE/84-1, revised 1987.

[23] H. Fesefeldt, RWTH Aachen, Report PITHA 85/02 (1985).

[24] GRC4F version 2.1 is used.
J. Fujimoto *et al.*, Comp. Phys. Comm. **100** (1997) 128.

[25] Miroslav Kopal, *Measurements of four fermion cross-sections at LEP*, Ph.D. thesis, Purdue University, 2002;
Gagan Mohanty, *Study of Z-Boson Pair Production and Search for Physics beyond Standard Model at LEP-II*, Ph.D. thesis, University of Mumbai, 2002.

[26] S. Bethke *et al.*, Nucl. Phys. **B 370** (1992) 310.

The L3 Collaboration:

P.Achard,[20] O.Adriani,[17] M.Aguilar-Benitez,[25] J.Alcaraz,[25] G.Alemanni,[23] J.Allaby,[18] A.Aloisio,[29] M.G.Alviggi,[29] H.Anderhub,[49] V.P.Andreev,[6,34] F.Anselmo,[8] A.Arefiev,[28] T.Azemoon,[3] T.Aziz,[9] P.Bagnaia,[39] A.Bajo,[25] G.Baksay,[26] L.Baksay,[26] S.V.Baldew,[2] S.Banerjee,[9] Sw.Banerjee,[4] A.Barczyk,[49,47] R.Barillère,[18] P.Bartalini,[23] M.Basile,[8] N.Batalova,[46] R.Battiston,[33] A.Bay,[23] F.Becattini,[17] U.Becker,[13] F.Behner,[49] L.Bellucci,[17] R.Berbeco,[3] J.Berdugo,[25] P.Berges,[13] B.Bertucci,[33] B.L.Betev,[49] M.Biasini,[33] M.Biglietti,[29] A.Biland,[49] J.J.Blaising,[4] S.C.Blyth,[35] G.J.Bobbink,[2] A.Böhm,[1] L.Boldizsar,[12] B.Borgia,[39] S.Bottai,[17] D.Bourilkov,[49] M.Bourquin,[20] S.Braccini,[20] J.G.Branson,[41] F.Brochu,[4] J.D.Burger,[13] W.J.Burger,[33] X.D.Cai,[13] M.Capell,[13] G.Cara Romeo,[8] G.Carlino,[29] A.Cartacci,[17] J.Casaus,[25] F.Cavallari,[39] N.Cavallo,[36] C.Cecchi,[33] M.Cerrada,[25] M.Chamizo,[20] Y.H.Chang,[44] M.Chemarin,[24] A.Chen,[44] G.Chen,[7] G.M.Chen,[7] H.F.Chen,[22] H.S.Chen,[7] G.Chiefari,[29] L.Cifarelli,[40] F.Cindolo,[8] I.Clare,[13] R.Clare,[38] G.Coignet,[4] N.Colino,[25] S.Costantini,[39] B.de la Cruz,[25] S.Cucciarelli,[33] R.de Asmundis,[29] P.Déglon,[20] J.Debreczeni,[12] A.Degré,[4] K.Dehmelt,[26] K.Deiters,[47] D.della Volpe,[29] E.Delmeire,[20] P.Denes,[37] F.DeNotaristefani,[39] A.De Salvo,[49] M.Diemoz,[39] M.Dierckxsens,[2] C.Dionisi,[39] M.Dittmar,[49] A.Doria,[29] M.T.Dova,[10,♯] D.Duchesneau,[4] M.Duda,[1] B.Echenard,[20] A.Eline,[18] A.El Hage,[1] H.El Mamouni,[24] A.Engler,[35] F.J.Eppling,[13] P.Extermann,[20] M.A.Falagan,[25] S.Falciano,[39] A.Favara,[32] J.Fay,[24] O.Fedin,[34] M.Felcini,[49] T.Ferguson,[35] H.Fesefeldt,[1] E.Fiandrini,[33] J.H.Field,[20] F.Filthaut,[31] P.H.Fisher,[13] W.Fisher,[37] I.Fisk,[41] G.Forconi,[13] K.Freudenreich,[49] C.Furetta,[27] Yu.Galaktionov,[28,13] S.N.Ganguli,[9] P.Garcia-Abia,[25] M.Gataullin,[32] S.Gentile,[39] S.Giagu,[39] Z.F.Gong,[22] G.Grenier,[24] O.Grimm,[49] M.W.Gruenewald,[16] M.Guida,[40] V.K.Gupta,[37] A.Gurtu,[9] L.J.Gutay,[46] D.Haas,[5] D.Hatzifotiadou,[8] T.Hebbeker,[1] A.Hervé,[18] J.Hirschfelder,[35] H.Hofer,[49] M.Hohlmann,[26] G.Holzner,[49] S.R.Hou,[44] B.N.Jin,[7] P.Jindal,[14] L.W.Jones,[3] P.de Jong,[2] I.Josa-Mutuberría,[25] M.Kaur,[14] M.N.Kienzle-Focacci,[20] J.K.Kim,[43] J.Kirkby,[18] W.Kittel,[31] A.Klimentov,[13,28] A.C.König,[31] M.Kopal,[46] V.Koutsenko,[13,28] M.Kräber,[49] R.W.Kraemer,[35] A.Krüger,[48] A.Kunin,[13] P.Ladron de Guevara,[25] I.Laktineh,[24] G.Landi,[17] M.Lebeau,[18] A.Lebedev,[13] P.Lebrun,[24] P.Lecomte,[49] P.Lecoq,[18] P.Le Coultre,[49] J.M.Le Goff,[18] R.Leiste,[48] M.Levtchenko,[27] P.Levtchenko,[34] C.Li,[22] S.Likhoded,[48] C.H.Lin,[44] W.T.Lin,[44] F.L.Linde,[2] L.Lista,[29] Z.A.Liu,[7] W.Lohmann,[48] E.Longo,[39] Y.S.Lu,[7] C.Luci,[39] L.Luminari,[39] W.Lustermann,[49] W.G.Ma,[22] L.Malgeri,[18] A.Malinin,[28] C.Maña,[25] J.Mans,[37] J.P.Martin,[24] F.Marzano,[39] K.Mazumdar,[9] R.R.McNeil,[6] S.Mele,[18,29] L.Merola,[29] M.Meschini,[17] W.J.Metzger,[31] A.Mihul,[11] H.Milcent,[18] G.Mirabelli,[39] J.Mnich,[1] G.B.Mohanty,[9] G.S.Muanza,[24] A.J.M.Muijs,[2] B.Musicar,[41] M.Musy,[39] S.Nagy,[15] S.Natale,[20] M.Napolitano,[29] F.Nessi-Tedaldi,[49] H.Newman,[32] A.Nisati,[39] T.Novak,[31] H.Nowak,[48] R.Ofierzynski,[49] G.Organtini,[39] I.Pal,[46] C.Palomares,[25] P.Paolucci,[29] R.Paramatti,[39] G.Passaleva,[17] S.Patricelli,[29] T.Paul,[10] M.Pauluzzi,[33] C.Paus,[13] F.Pauss,[49] M.Pedace,[39] S.Pensotti,[27] D.Perret-Gallix,[4] D.Piccolo,[29] F.Pierella,[8] M.Pioppi,[33] P.A.Piroué,[37] E.Pistolesi,[27] V.Plyaskin,[28] M.Pohl,[20] V.Pojidaev,[17] J.Pothier,[18] D.Prokofiev,[34] G.Rahal-Callot,[49] M.A.Rahaman,[9] P.Raics,[15] N.Raja,[9] R.Ramelli,[49] P.G.Rancoita,[27] R.Ranieri,[17] A.Raspereza,[48] P.Razis,[30] D.Ren,[49] M.Rescigno,[39] S.Reucroft,[10] S.Riemann,[48] K.Riles,[3] B.P.Roe,[3] L.Romero,[25] A.Rosca,[48] C.Rosemann,[1] C.Rosenbleck,[1] S.Rosier-Lees,[4] S.Roth,[1] B.Roux,[31] J.A.Rubio,[18] G.Ruggiero,[17] H.Rykaczewski,[49] A.Sakharov,[49] S.Saremi,[6] S.Sarkar,[39] J.Salicio,[18] E.Sanchez,[25] C.Schäfer,[18] V.Schegelsky,[34] H.Schopper,[21] D.J.Schotanus,[31] C.Sciacca,[29] L.Servoli,[33] S.Shevchenko,[32] N.Shivarov,[42] V.Shoutko,[13] E.Shumilov,[28] A.Shvorob,[32] D.Son,[43] C.Souga,[24] P.Spillantini,[17] M.Steuer,[13] D.P.Stickland,[37] B.Stoyanov,[42] A.Straessner,[20] K.Sudhakar,[9] G.Sultanov,[42] L.Z.Sun,[22] S.Sushkov,[1] H.Suter,[49] J.D.Swain,[10] Z.Szillasi,[26,¶] X.W.Tang,[7] P.Tarjan,[15] L.Tauscher,[5] L.Taylor,[10] B.Tellili,[24] D.Teyssier,[24] C.Timmermans,[31] Samuel C.C.Ting,[13] S.M.Ting,[13] S.C.Tonwar,[9] J.Tóth,[12] C.Tully,[37] K.L.Tung,[7] J.Ulbricht,[49] E.Valente,[39] R.T.Van de Walle,[31] R.Vasquez,[46] V.Veszpremi,[26] G.Vesztergombi,[12] I.Vetlitsky,[28] G.Viertel,[49] S.Villa,[38] M.Vivargent,[4] S.Vlachos,[5] I.Vodopianov,[26] H.Vogel,[35] H.Vogt,[48] I.Vorobiev,[35,28] A.A.Vorobyov,[34] M.Wadhwa,[5] Q.Wang,[31] X.L.Wang,[22] Z.M.Wang,[22] M.Weber,[18] S.Wynhoff,[37] L.Xia,[32] Z.Z.Xu,[22] J.Yamamoto,[3] B.Z.Yang,[22] C.G.Yang,[7] H.J.Yang,[3] M.Yang,[7] S.C.Yeh,[45] An.Zalite,[34] Yu.Zalite,[34] Z.P.Zhang,[22] J.Zhao,[22] G.Y.Zhu,[7] R.Y.Zhu,[32] H.L.Zhuang,[7] A.Zichichi,[8,18,19] B.Zimmermann,[49] M.Zöller.[1]

1 III. Physikalisches Institut, RWTH, D-52056 Aachen, Germany[§]
2 National Institute for High Energy Physics, NIKHEF, and University of Amsterdam, NL-1009 DB Amsterdam, The Netherlands
3 University of Michigan, Ann Arbor, MI 48109, USA
4 Laboratoire d'Annecy-le-Vieux de Physique des Particules, LAPP,IN2P3-CNRS, BP 110, F-74941 Annecy-le-Vieux CEDEX, France
5 Institute of Physics, University of Basel, CH-4056 Basel, Switzerland
6 Louisiana State University, Baton Rouge, LA 70803, USA
7 Institute of High Energy Physics, IHEP, 100039 Beijing, China[△]
8 University of Bologna and INFN-Sezione di Bologna, I-40126 Bologna, Italy
9 Tata Institute of Fundamental Research, Mumbai (Bombay) 400 005, India
10 Northeastern University, Boston, MA 02115, USA
11 Institute of Atomic Physics and University of Bucharest, R-76900 Bucharest, Romania
12 Central Research Institute for Physics of the Hungarian Academy of Sciences, H-1525 Budapest 114, Hungary[‡]
13 Massachusetts Institute of Technology, Cambridge, MA 02139, USA
14 Panjab University, Chandigarh 160 014, India
15 KLTE-ATOMKI, H-4010 Debrecen, Hungary[¶]
16 Department of Experimental Physics, University College Dublin, Belfield, Dublin 4, Ireland
17 INFN Sezione di Firenze and University of Florence, I-50125 Florence, Italy
18 European Laboratory for Particle Physics, CERN, CH-1211 Geneva 23, Switzerland
19 World Laboratory, FBLJA Project, CH-1211 Geneva 23, Switzerland
20 University of Geneva, CH-1211 Geneva 4, Switzerland
21 University of Hamburg, D-22761 Hamburg, Germany
22 Chinese University of Science and Technology, USTC, Hefei, Anhui 230 029, China[△]
23 University of Lausanne, CH-1015 Lausanne, Switzerland
24 Institut de Physique Nucléaire de Lyon, IN2P3-CNRS,Université Claude Bernard, F-69622 Villeurbanne, France
25 Centro de Investigaciones Energéticas, Medioambientales y Tecnológicas, CIEMAT, E-28040 Madrid, Spain[♭]
26 Florida Institute of Technology, Melbourne, FL 32901, USA
27 INFN-Sezione di Milano, I-20133 Milan, Italy
28 Institute of Theoretical and Experimental Physics, ITEP, Moscow, Russia
29 INFN-Sezione di Napoli and University of Naples, I-80125 Naples, Italy
30 Department of Physics, University of Cyprus, Nicosia, Cyprus
31 Radboud University and NIKHEF, NL-6525 ED Nijmegen, The Netherlands
32 California Institute of Technology, Pasadena, CA 91125, USA
33 INFN-Sezione di Perugia and Università Degli Studi di Perugia, I-06100 Perugia, Italy
34 Nuclear Physics Institute, St. Petersburg, Russia
35 Carnegie Mellon University, Pittsburgh, PA 15213, USA
36 INFN-Sezione di Napoli and University of Potenza, I-85100 Potenza, Italy
37 Princeton University, Princeton, NJ 08544, USA
38 University of Californa, Riverside, CA 92521, USA
39 INFN-Sezione di Roma and University of Rome, "La Sapienza", I-00185 Rome, Italy
40 University and INFN, Salerno, I-84100 Salerno, Italy
41 University of California, San Diego, CA 92093, USA
42 Bulgarian Academy of Sciences, Central Lab. of Mechatronics and Instrumentation, BU-1113 Sofia, Bulgaria
43 The Center for High Energy Physics, Kyungpook National University, 702-701 Taegu, Republic of Korea
44 National Central University, Chung-Li, Taiwan, China
45 Department of Physics, National Tsing Hua University, Taiwan, China
46 Purdue University, West Lafayette, IN 47907, USA
47 Paul Scherrer Institut, PSI, CH-5232 Villigen, Switzerland
48 DESY, D-15738 Zeuthen, Germany
49 Eidgenössische Technische Hochschule, ETH Zürich, CH-8093 Zürich, Switzerland
§ Supported by the German Bundesministerium für Bildung, Wissenschaft, Forschung und Technologie.
‡ Supported by the Hungarian OTKA fund under contract numbers T019181, F023259 and T037350.
¶ Also supported by the Hungarian OTKA fund under contract number T026178.
♭ Supported also by the Comisión Interministerial de Ciencia y Tecnología.
♯ Also supported by CONICET and Universidad Nacional de La Plata, CC 67, 1900 La Plata, Argentina.
△ Supported by the National Natural Science Foundation of China.

$\sqrt{s}$ [GeV]	182.7	188.6	191.6	195.5	199.5	201.7	205.1	206.8	196.6
$\mathcal{L}$ [pb^{-1}]	55.4	176.8	29.7	83.7	82.7	37.1	69.1	138.9	673.4

Table 2: Centre-of-mass energies and integrated luminosities for the different data-taking periods. The last column gives the luminosity-averaged centre-of-mass energy and the total integrated luminosity.

$e^+e^- \to$	$N_{\rm Data}$	$N^{\rm MC}_{\rm Sign}$	$N^{\rm MC}_{\rm Back}$	ε	σ_{4f} [pb]	$\sigma^{\rm Th}_{4f}$ [pb]
$q\bar{q}\nu\bar{\nu}$	198	73.2	125.8	38.1 %	$0.278 \pm 0.052 \pm 0.021$	0.282
$q\bar{q}e^+e^-$	109	60.4	37.8	59.1 %	$0.156 \pm 0.022 \pm 0.006$	0.127
$q\bar{q}\mu^+\mu^-$	38	30.8	9.4	52.8 %	$0.073 \pm 0.016 \pm 0.003$	0.082
$\ell^+\ell^-\nu\bar{\nu}$	17	7.0	7.4	28.7 %	$0.045 \pm 0.022 \pm 0.004$	0.036
$\ell^+\ell^-\ell'^+\ell'^-$	25	14.8	9.9	39.9 %	$0.058 \pm 0.018 \pm 0.004$	0.054

Table 3: Numbers of events observed for the $e^+e^- \to f\bar{f}f'\bar{f}'$ selections, $N_{\rm Data}$, compared to the Monte Carlo predictions for signal, $N^{\rm MC}_{\rm Sign}$, and background, $N^{\rm MC}_{\rm Back}$. The selection efficiencies, ε, are also given together with the measured cross sections, σ_{4f} and the expectations from the GRC4F Monte Carlo, $\sigma^{\rm Th}_{4f}$. They refer to the luminosity-weighted average of the cross sections for each value of $\sqrt{s}$ in Table 2, corresponding to an average centre-of-mass energy $< \sqrt{s} >= 196.6$ GeV. The first uncertainty on σ_{4f} is statistical and the second systematic.

$e^+e^- \to Z\gamma^* \to$	$N_{\rm Data}$	$N^{\rm MC}_{\rm Sign}$	$N^{\rm MC}_{\rm Back}$	ε	$\sigma_{Z\gamma^*}$ [pb]	$\sigma^{\rm Th}_{Z\gamma^*}$ [pb]
$q\bar{q}\nu\bar{\nu}$	198	17.9	181.1	31.7 %	$0.072 \pm 0.044 \pm 0.017$	0.083
$q\bar{q}e^+e^-$	109	23.5	74.7	58.8 %	$0.100 \pm 0.023 \pm 0.007$	0.059
$q\bar{q}\mu^+\mu^-$	38	14.0	26.3	49.2 %	$0.040 \pm 0.017 \pm 0.004$	0.042
$\ell^+\ell^-\nu\bar{\nu}$	17	3.2	11.3	27.5 %	$0.039 \pm 0.020 \pm 0.004$	0.017
$\ell^+\ell^-\ell'^+\ell'^-$	25	5.3	19.5	45.7 %	$0.019 \pm 0.015 \pm 0.004$	0.017
$f\bar{f}f'\bar{f}'$	387	63.9	312.6	43.2 %	$0.288 \pm 0.052 \pm 0.031$	0.218

Table 4: Numbers of events observed for the $e^+e^- \to Z\gamma^* \to f\bar{f}f'\bar{f}'$ selections, $N_{\rm Data}$, compared to the Monte Carlo predictions for signal, $N^{\rm MC}_{\rm Sign}$, and background, $N^{\rm MC}_{\rm Back}$. The selection efficiencies, ε, are also given together with the measured cross sections, $\sigma_{Z\gamma^*}$ and the expectations from the GRC4F Monte Carlo, $\sigma^{\rm Th}_{Z\gamma^*}$. They refer to the luminosity-weighted average of the cross sections for each value of $\sqrt{s}$ in Table 2, corresponding to an average centre-of-mass energy $< \sqrt{s} >= 196.6$ GeV. The first uncertainty on $\sigma_{Z\gamma^*}$ is statistical and the second systematic.

	$q\bar{q}e^+e^-$		$q\bar{q}\mu^+\mu^-$		$q\bar{q}\nu\bar{\nu}$		$\ell^+\ell^-\nu\bar{\nu}$		$\ell^+\ell^-\ell'^+\ell'^-$		Comb.
Source	$4f$	$Z\gamma^*$	$4f$	$Z\gamma^*$	$4f$	$Z\gamma^*$	$4f$	$Z\gamma^*$	$4f$	$Z\gamma^*$	$Z\gamma^*$
Energy scale	0.7	0.7	0.7	0.7	3.6	3.6	—	—	—	—	1.1
Lepton identification	1.9	1.9	1.9	1.9	—	—	0.8	0.8	0.7	0.7	1.4
Cut variation	2.2	2.2	2.2	2.2	3.6	3.6	4.8	4.8	4.6	4.6	2.7
MC statistics (sign.)	0.6	0.6	0.5	0.2	0.2	0.3	0.4	0.7	0.4	0.5	0.5
MC statistics (back.)	2.2	2.2	3.4	3.5	0.7	0.7	<0.1	0.7	<0.1	0.3	2.4
Background normalisation	1.5	6.8	0.5	8.4	5.6	22.4	8.2	8.6	5.7	19.2	9.9
Total	4.0	7.8	4.6	9.6	7.6	23.0	9.5	9.9	7.4	19.8	10.7

Table 5: Sources and effects of systematic uncertainties. Values are given as the percentual variation on the measured cross sections of the $e^+e^- \to f\bar{f}f'\bar{f}'$ ($4f$) and $e^+e^- \to Z\gamma^* \to f\bar{f}f'\bar{f}'$ ($Z\gamma^*$) processes. The last column refers to the combination of the channels used to measure the $e^+e^- \to Z\gamma^* \to f\bar{f}f'\bar{f}'$ cross section. The total systematic uncertainty is the sum in quadrature of the different contributions.

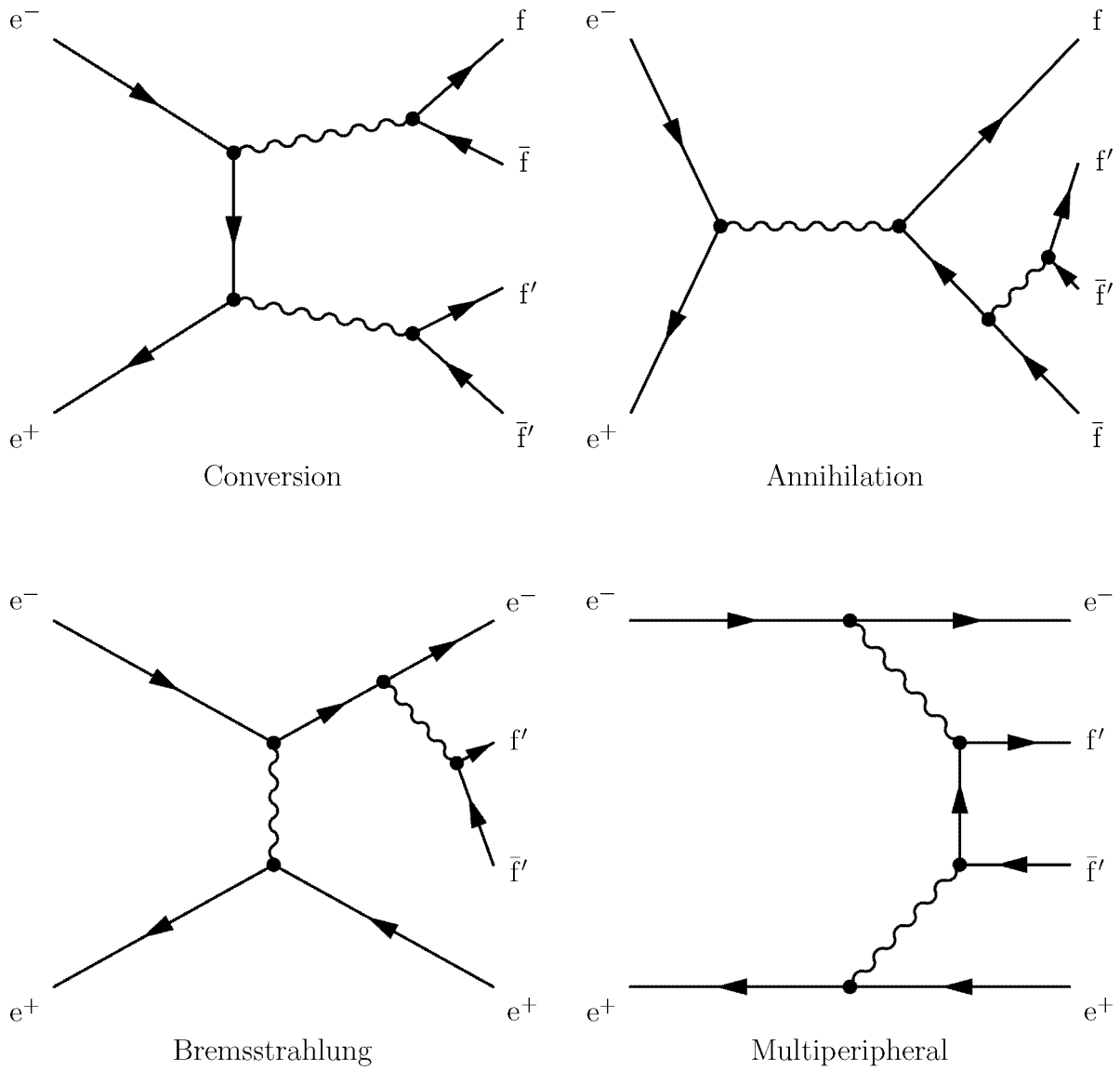

Figure 1: Dominant Feynman diagrams contributing to neutral-current four-fermion production. The wavy lines represent a Z boson or an off-mass-shell photon.

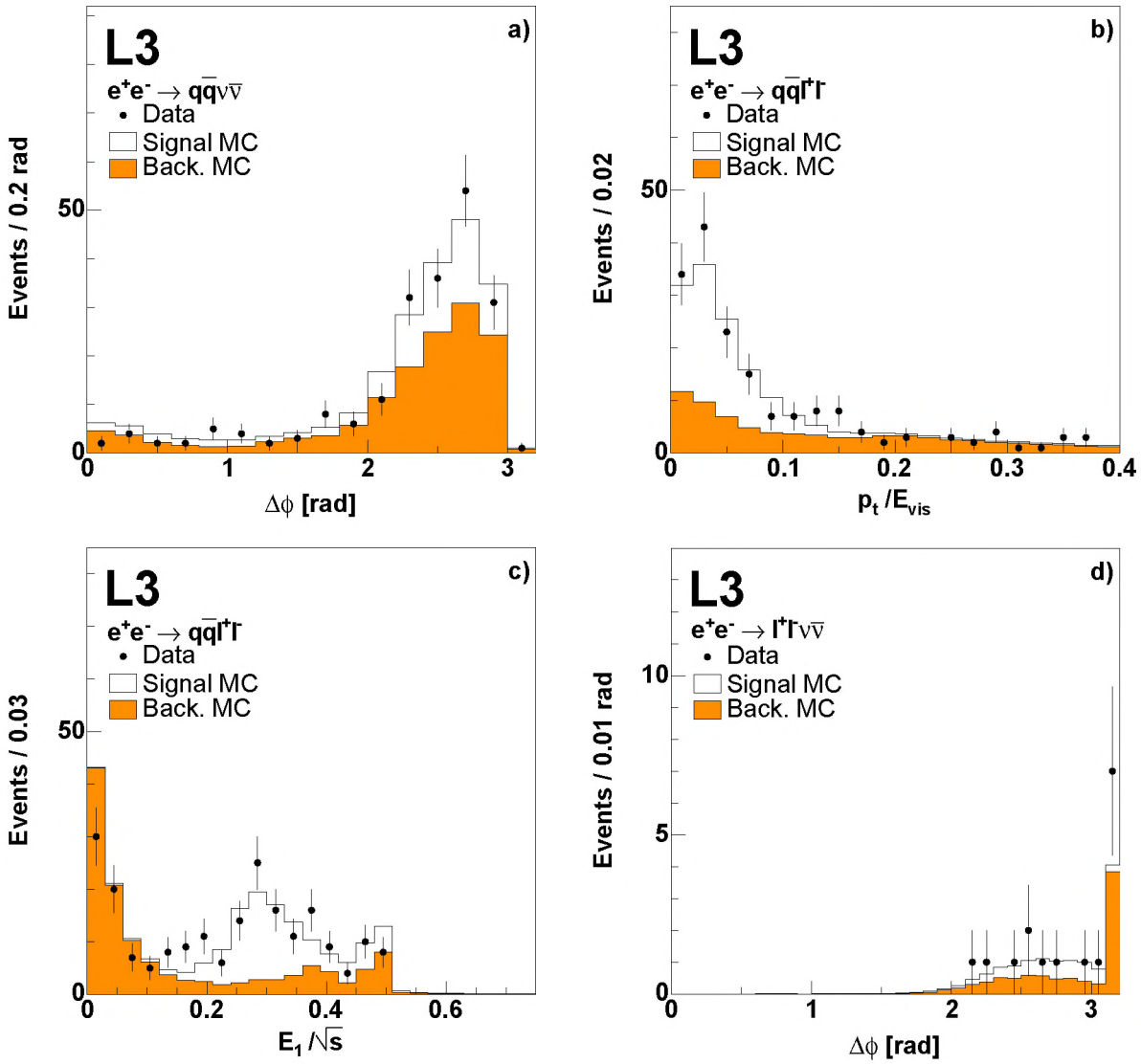

Figure 2: Distribution of selection variables for the different channels. a) The angle in the plane transverse to the beams for the two jets of the $q\bar{q}\nu\bar{\nu}$ channel, b) the transverse momentum normalised to the visible energy for the $q\bar{q}\ell^+\ell^-$ channel, c) the energy of the most energetic lepton normalised to $\sqrt{s}$ for the $q\bar{q}\ell^+\ell^-$ channel and d) the angle in the plane transverse to the beams for the two leptons of the $\ell^+\ell^-\nu\bar{\nu}$ channel. In each plot, all selection cuts are applied with the exception of that on the shown variable.

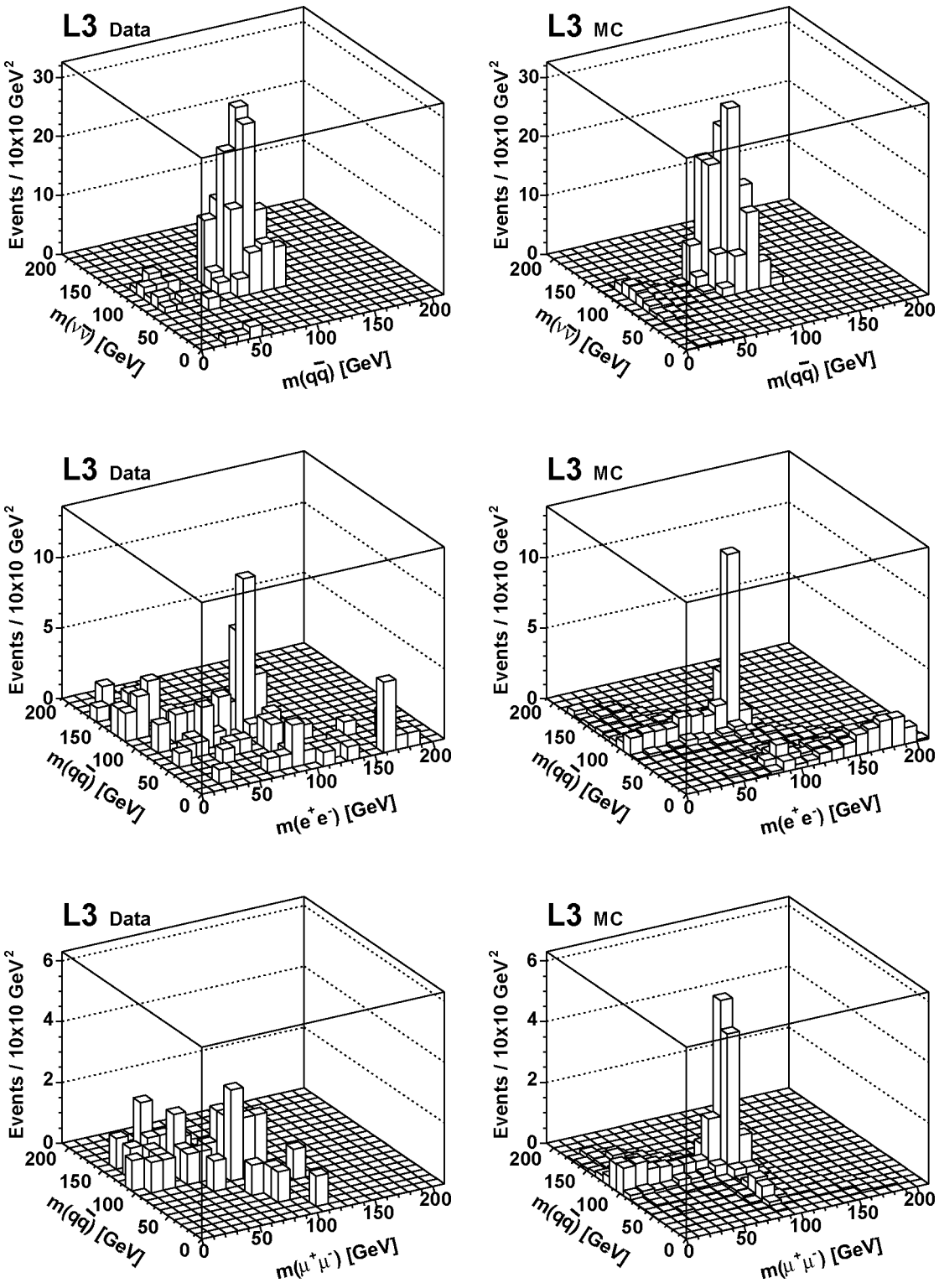

Figure 3: Distributions of the missing mass *vs.* the hadron mass for the $q\bar{q}\nu\bar{\nu}$ channel, first row, and the lepton mass *vs.* the hadron mass for the $q\bar{q}e^+e^-$ channel, second row, and $q\bar{q}\mu^+\mu^-$ channel, third row. The left-hand side plots represent the data, the right-hand side ones the Monte Carlo predictions.

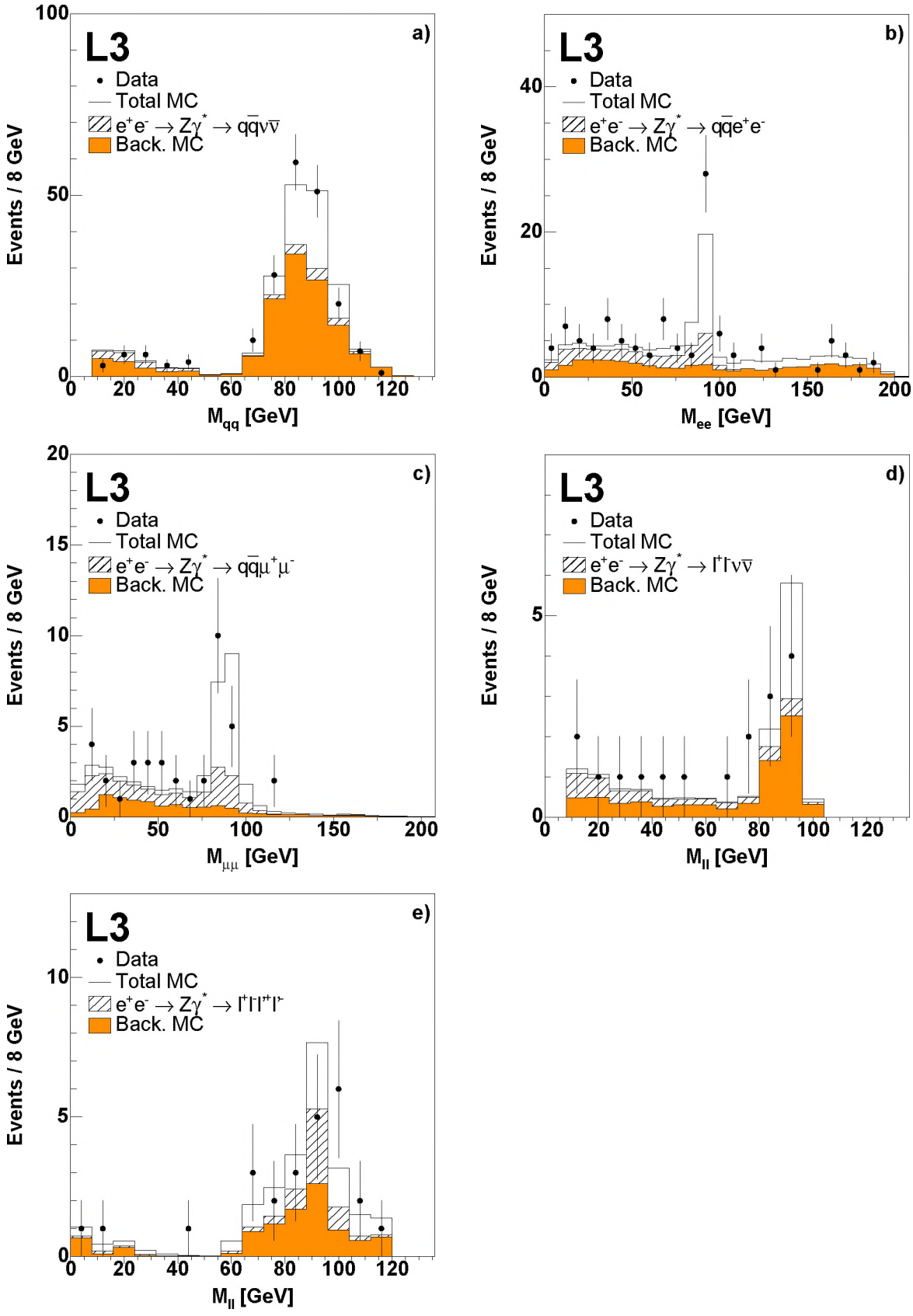

Figure 4: Distributions of a) the mass of the hadron system in the $q\bar{q}\nu\bar{\nu}$ channel; the mass of the lepton pair in the b) $q\bar{q}e^+e^-$ c) $q\bar{q}\mu^+\mu^-$ and d) $\ell^+\ell^-\nu\bar{\nu}$ channels and e) the mass of the selected lepton pair in the $\ell^+\ell^-\ell'^+\ell'^-$ channel.

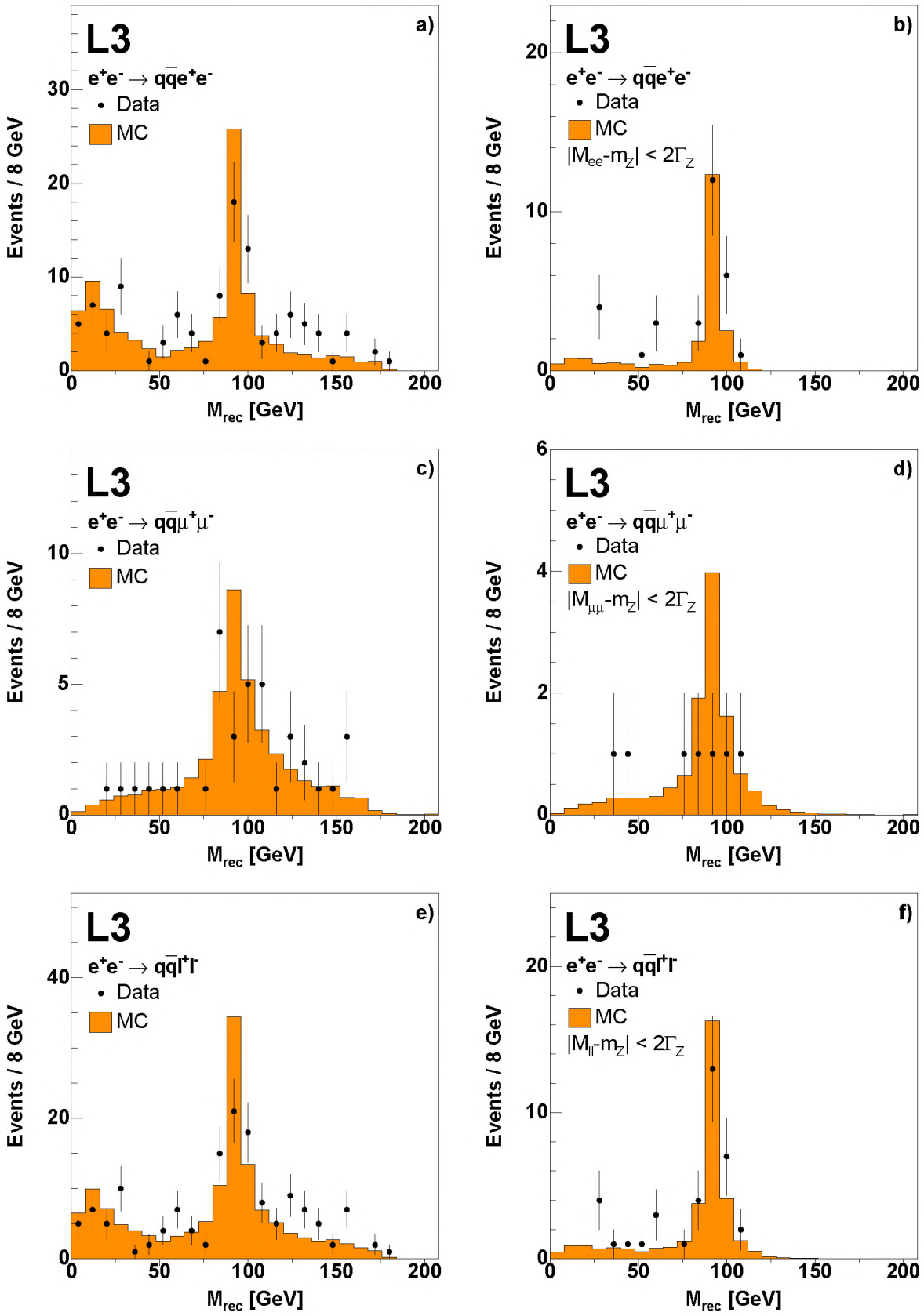

Figure 5: Distribution of the recoil mass to the lepton system for the a) $q\bar{q}e^+e^-$ and c) $q\bar{q}\mu^+\mu^-$ channels with e) their sum. Figures b), d) and f) show the same variables as a), c) and e), respectively, if a cut $|m_{\ell\ell} - m_Z| < 2\Gamma_Z$ is applied on the lepton mass.

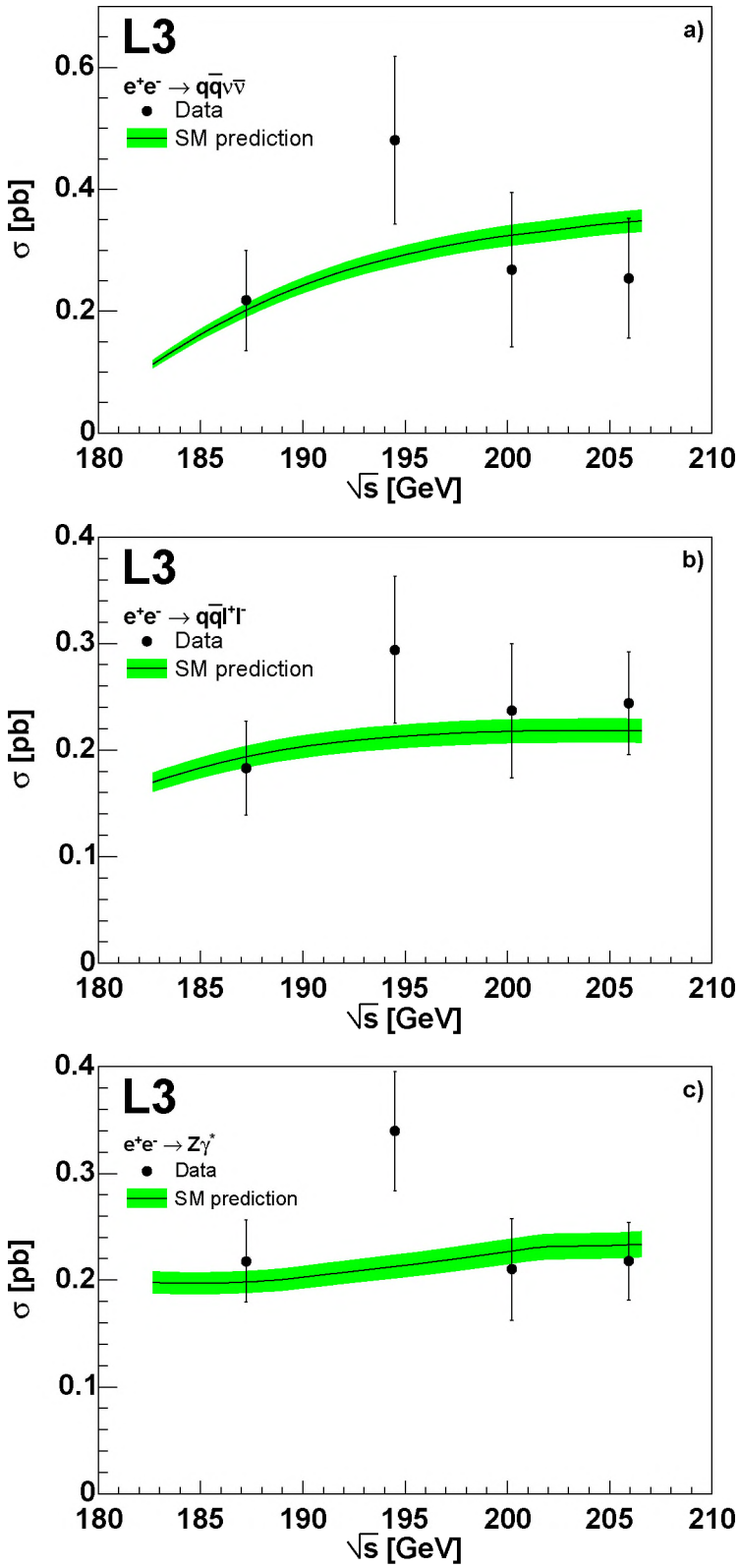

Figure 6: Cross sections measured as a function of the centre-of-mass energies for the a) $e^+e^- \to q\bar{q}\nu\bar{\nu}$, b) $e^+e^- \to q\bar{q}\ell^+\ell^-$ and c) $e^+e^- \to Z\gamma^* \to f\bar{f}f'\bar{f}'$ processes. The expectations from the GRC4F Monte Carlo are also shown, with an uncertainty of ±5%. Both the data and the predictions for the $e^+e^- \to q\bar{q}\ell^+\ell^-$ process refer to the sum of the electron and muon final states.